

## **Comparison Between the Influence of Mechanical and Electromagnetic Stirring on Aluminum Ingot Purity During Ohno Continuous Casting**

**S. Fashu<sup>1\*</sup>, M.Tozvireva<sup>1</sup>, L.Mudzingwa<sup>1</sup>, R.Khan<sup>2</sup> and A. Mukuya<sup>1</sup>**

**Abstract** This paper outlines the findings in the comparison of the influence of mechanical and electromagnetic stirring on ingot long term purity and uniformity during Ohno Continuous Casting. The magnitude of the average optimum velocity flow field and stirring parameters required to effectively purify aluminum ingots using mechanical stirring of the melt was determined and analyzed. Basing on the determined optimum mechanical flow field, electromagnetic parameters producing almost the same flow field near the interface were obtained through careful adjustments of parameters. Optimum parameters of the mechanical and electromagnetic stirring were obtained by numerically solving the solidification model coupled with either the multi-reference frame model (for mechanical stirring) or the magnetohydrodynamic model (for electromagnetic stirring) in CFD Fluent 6.3.26 software. For mechanical stirring, an optimum stirring intensity of 2mm/min was determined whilst for electromagnetic stirring, the optimum magnetic field with an amplitude of 20mT and a frequency of 2.7Hz was determined and these produced same magnitude optimum flow fields resulting in high purity aluminum ingots. Comparison of the two methods showed that electromagnetic stirring is good in covering all the regions near the solid-liquid interface and is more effective in bulk melt mixing; thus produces more uniform and purer ingots for longer casting times.

**Keywords:** Electromagnetic field, computer simulation, convection, interface, stirring.

---

<sup>1</sup> Department of Materials Science and Technology, Harare Institute of Technology, Harare, Zimbabwe.

<sup>2</sup> Department of Physics, Abdul Wali Khan University, Mardan, 23200 KPK Pakistan.

\* Corresponding author: Tel./fax: +263-4-741430, E-mail address: sfashu04@gmail.com

## **1 Introduction**

From the past three decades, high purity aluminum rods of superior quality are being produced by the Ohno continuous casting (OCC) process as shown by Ohno (1986), Wang (2015) and Motoyasu (2015). They are in high demand in the optoelectronics industry for audio and video cables applications as shown by Okoyasu (2010). Ohno continuous casting process is a heated mould system that permits the production of net-shape or near-net-shape products with a high-quality surface, controlled solidification structure, and significantly enhanced properties. The detailed description of the OCC technology is given by Ohno (1986) and Motoyasu (2015). According to Tiller (1953), a solute boundary layer is accumulated at the solidification front during OCC casting because of segregation of different elements in the liquid or solid phase and this solute rich interface reduces the purity of the alloy ingot. A sufficiently strong convection in the melt towards the solidification front reduces the thickness of the boundary layer and purifies the ingot as shown by Tiller (1953) and Shingu (1983). The mechanism of purification involves breaking down dendrites extending from the liquid-solid interface into the liquid phase to release impurities from between the dendrites or between the branches of the dendrites, and dispersing the released impurities in the entire body of the liquid phase. This technique purifies ingots since the solute impurities will be continuously ejected from a solidifying ingot and transported into the bulk melt preventing back diffusion into the solid as demonstrated by Shingu (1983).

Several methods are known for inducing forced convection in the melt during solidification and mainly include ultrasonic, mechanical and electromagnetic stirring. Among the known melt forced stirring techniques, electromagnetic stirring (EMS) is, perhaps, the most popular one as it is non-intrusive/contactless, offers direct and simple control of flow intensity through adjusting magnetic field parameters, thus producing efficient uniform stirring and desired heat and mass transport as demonstrated by Willers (2008) and Eckert (2007). This purifying technique of using electromagnetic stirring is now well established in purification of silicon containing trace impurities and this was observed by Jie (2014), Yu (2014), Ban (2015), Yu (2017) and Cablea (2015). Thus, control of solute transport and ingot properties with electromagnetic stirring is widely adopted in the field of solidification processing using various magnetic fields such as the fixed alternating magnetic field at induction heating, the high gradient magnetic field and the rotating magnetic field. Mullin (1958) observed that by applying rotating magnetic fields during zone refining, the diffusive boundary layer at the solidification interface can be reduced. Many researchers including Li (2007), Mitric (2008) and Zeng (2016) investigated the effect of electromagnetic parameters and stirrer design, intensity,

frequency, location, length and orientation on various properties of produced ingots including purity and homogeneity. Using the numerical solution of magnetohydrodynamic (MHD) model, Marcelo (2003) and Marcelo (2007) devised a constrained optimization algorithm that is capable of automatically determining the correct strengths, locations, and orientations of a finite number of magnets to produce the magnetic field force pattern that will create the specified concentration pattern in the fluid. Besides electromagnetic stirring, mechanical melt stirring using specially designed stirrers is a promising and competing technique since it is was shown to be a simple, cheap and easy to use process by Shingu (1983), Dumitrica (2012) and Fashu (2011). Thus, it is interesting to compare and contrast the influence of electromagnetic and mechanical stirring on ingot purity and evaluate the differences as a guide to operators. The influence of melt stirring on alloys grain refinement received a considerable attention including that from Metan (2009), Li (2016) and Mapelli (2010), but research of purification using stirring is still scarce except for silicon refinement. Most of researches on purification of alloys during solidification are on purification of silicon for solar photovoltaic applications.

In this work, first, the optimum mechanical stirring velocity and resulting solute and flow fields required to eliminate the solute boundary layer are determined. Then basing on the obtained velocity flow fields, the optimum magnetic field parameters (strength and frequency) required to produce the same magnitude velocity flow fields were computed. The numerical optimization of the mechanical stirrer rotation speed and magnetic field parameters was performed using the CFD Fluent 6.3.26 software. Subsequently a comparison of the influence of mechanical and electromagnetic stirring on ingot long term purity and uniformity was done.

## **2 Solidification model**

The governing equations based on the continuum formulation of Benon (1987) were solved with the aid of User Defined Subroutines in CFD Fluent 6.3.26 software.

### ***2.1 Assumptions***

- i. All of the properties of the mixture can be obtained from the properties of its individual components in each phase.
- ii. All transport properties of each phase, such as thermal and electrical conductivity or viscosity are constants.
- iii. The densities are constant in each phase.

- iv. The mushy region is modeled by means of using the mixture viscosity.
- v. Local equilibrium is assumed to exist at the solid-liquid interface i.e. the phase diagram applies.
- vi. The flow of the liquid phase is assumed incompressible, laminar and Newtonian.
- vii. Solutes diffusion coefficients are isotropic and constant in each phase.
- viii. The electromagnetic characteristics of the melt are isotropic and uniform.

Based on the assumptions made above, the set of governing equations of mass, momentum, energy and solute are formulated as:

### **2.2 Mass conservation equation**

$$\frac{\partial \rho}{\partial t} + \nabla \cdot (\rho \vec{u}) = 0 \quad (1)$$

Where  $\rho$  is the density,  $\vec{u}$  is the velocity vector.

### **2.3 Momentum conservation equation**

$$\frac{\partial (\rho \vec{u})}{\partial t} + \nabla \cdot (\rho \vec{u} \vec{u}) = -\nabla p + \nabla \cdot (\mu_l \nabla \vec{u}) - \frac{\mu_l}{K} \vec{u} + S_m \quad (2)$$

Where  $p$  is the pressure,  $\mu_l$  is the dynamic viscosity of the melt,  $K$  is the permeability constant of the mushy zone and  $S_m$  is the momentum source which can be either due to mechanical or magnetic stirring.

### **2.4 Energy conservation equation**

$$\frac{\partial (\rho H)}{\partial t} + \nabla \cdot (\rho H \vec{u}) = \nabla \cdot (k \nabla T) + S_h \quad (3)$$

Where  $H$  is the enthalpy,  $k$  is the thermal conductivity,  $T$  is the temperature and  $S_h$  is the source term due to heat released in the solid-liquid interface during solidification.

The liquid fraction is assumed to be linearly proportional to temperature as:

$$f_l = \begin{cases} 1 & \text{when } T \geq T_l \\ \frac{T - T_s}{T_l - T_s} & \text{when } T_l \geq T \geq T_s \\ 0 & \text{when } T \leq T_s \end{cases} \quad (4)$$

**2.5 Species mass conservation equation**

$$\frac{\partial(\rho C_i)}{\partial t} + \nabla \cdot (\rho [f_l \vec{u}_l C_{i,l} + (1 - f_l) \vec{u}_c C_{i,s}]) = \nabla \cdot [\rho f_l D_{i,m,l} \nabla C_{i,l} + (1 - f_l) \rho D_{i,m,s} \nabla C_{i,s}] - S_c \quad (5)$$

Where,  $C_i$  is the total mass fraction of species  $i$ ,  $C_i = f_s C_s + f_l C_l$ ,  $D$  is the diffusion coefficient,  $S_c$  is the source term governing the convective transport of solute rejected from the mushy zone. The subscripts  $i, l, c, m$  and  $s$  represents the species number, liquid, convection, mixture and solid respectively.

The mixture quantities are defined by the following auxiliary relationships:

$$f_l + f_s = 1, \quad H = H_L f_l + H_s f_s, \quad D = D_L f_l + D_s f_s, \quad k = k_l f_l + k_s f_s \quad (6)$$

With the assumption of local equilibrium, the energy and species conservation equations are closed using the equilibrium phase diagram.

**3 Mechanical stirring modeling**

**3.1 Model and implementation**

The OCC process is represented in Fig.1 and was simulated using the control volume based commercial CFD solver Fluent 6.3.26 software both in presence and absence of mechanical stirring. Pressure–velocity coupling was done with SIMPLE algorithm and pressure was discretized by the PRESTO! method. The ingot size used are of 58mm diameter and stirring was achieved through mechanical rotation of a stirrer propeller(43mmx4mm) positioned at approximately 30mm from the mold exit with the two dimensional domain of interest, as shown in Fig. 2. Momentum source terms due to mechanical stirring were introduced into the melt through Multiple Reference Frame (MRF) model and source terms of governing equations (energy and solute) were introduced through User Defined Functions (UDFs). Thermo-physical properties of the dilute industrial aluminum alloy together with the initial and boundary conditions used in the simulations are shown in Table 1 and Table 2 respectively. The typical dilute industrial aluminum alloy is composed of copper and silicon as major impurities which

are in small concentrations. The solid-liquid interface position was controlled to be near the stirring blades through adjustment of heat transfer coefficient of the water flux in the water spray region. Mechanical stirring was started after the process had reached steady state in order to allow the OCC process to quickly reach steady state. The optimum mechanical stirring rate was determined by increasing the stirring rate stepwise from zero and monitoring the ingot purity.

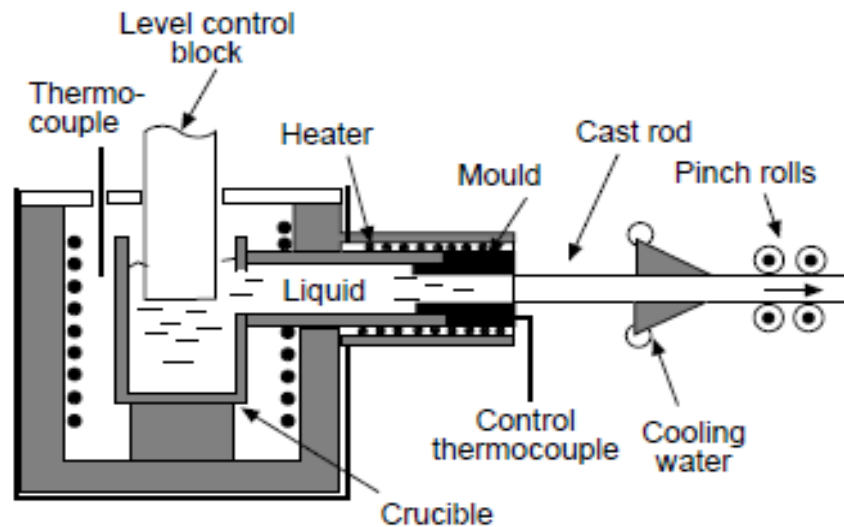


**Figure 1:** Schematic illustration of the Ohno continuous casting system showing casting of 58mm diameter ingots

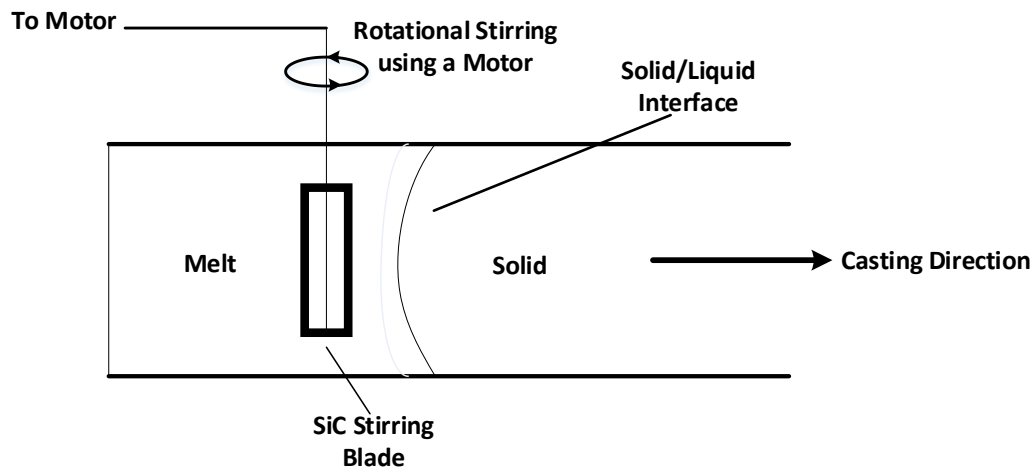


**Figure 2:** A stirrer positioned near the solid-liquid interface

**Table 1:** Thermo Physical Properties of Al-0.12wt%Cu-0.11 wt%Si alloy

<b>Property</b>	<b>Unit</b>	<b>Symbol</b>	<b>Value</b>
Density of Solid Al	kg/m <sup>3</sup>	$\rho_{Al(s)}$	2400
Density of Liquid Al	kg/m <sup>3</sup>	$\rho_{Al(l)}$	2700
Density of Solid Si	kg/m <sup>3</sup>	$\rho_{Si(s)}$	2329
Density of Liquid Si	kg/m <sup>3</sup>	$\rho_{Si(l)}$	2570
Density of Solid Cu	kg/m <sup>3</sup>	$\rho_{Cu(s)}$	8380
Density of Liquid Cu	kg/m <sup>3</sup>	$\rho_{Cu(l)}$	8020
Specific Heat	J/kgK	$C_p$	900
Thermal conductivity	w/mK	$K$	200
Thermal conductivity of Solid	w/mK	$K$	200
Diffusion Coefficient of Cu in Solid	m <sup>2</sup> /s	$D_s$	5e-13
Diffusion Coefficient of Cu in liquid	m <sup>2</sup> /s	$D_L$	6e-9
Diffusion Coefficient of Si in Solid	m <sup>2</sup> /s	$D_s$	1e-13
Diffusion Coefficient of Si in liquid	m <sup>2</sup> /s	$D_L$	5e-9
Melt Viscosity	Pas	$\mu$	1.3e-3
Partition coefficient of Cu in Al	-	$k$	0.14
Partition coefficient of Si in Al	-	$k$	0.13
Melting Heat	kJ	$L$	390
Melting point of Al		$T$	933
Slope of liquidus line, Al-Cu	-	$m$	-3.4
Slope of liquidus line, Al-Si	-	$m$	-6.2

**Table 2:** Initial and boundary conditions

<b>Property</b>	<b>Units</b>	<b>Value</b>
Nominal melt temperature	K	938
Heat transfer coefficient of Al in air	w/m <sup>2</sup> k	100
Heat transfer coefficient of Al in water spray	w/m <sup>2</sup> k	20000
Temperature of the heated mold	K	938

## 4 Electromagnetic stirring modeling

### 4.1 Configuration of the physical model

The arrangement of the electromagnetic stirrer position and orientation in the OCC mold is shown in Fig. 3. A given number of conducting coils with a given number of turns are stacked around the mold and near the solid-liquid interface in the electromagnetic stirrer. An alternating current with a given peak value of excitation current and frequency is passed through the solenoid coils that surround the heated mold to generate time varying magnetic field. The magnitude of the magnetic field depends upon the strength of the current and the number of turns in the coil.

The stirring is driven by the time dependent electromagnetic field that interacts with the induced current in the aluminum melt to generate the steady state Lorentz force field thereby inducing flow into the melt. The aim was to determine the magnetic field parameters required to produce the same velocity magnitudes in the melt as those produced by mechanical stirring illustrated in **Section 3** through proper parameters adjustments.

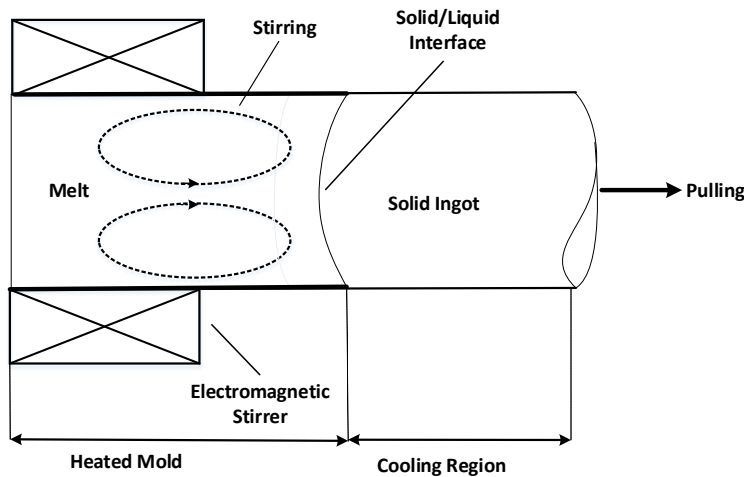


**Figure 3:** Schematic illustration of OCC process with electromagnetic stirrer

### 4.2 Numerical Model

The solidification problem with electromagnetic stirring was solved in CFD Fluent 6.3.26 finite volume code. The Lorentz forces and distribution of magnetic field in the aluminum melt were calculated by solving the magnetic induction equation derived from Ohm's Law and Maxwell's equations same as those used by Adler (2005) which is:

$$\frac{\partial \vec{B}}{\partial t} + (\vec{u} \cdot \nabla) \vec{B} = \frac{1}{\mu \sigma} \Delta \vec{B} + (\vec{B} \cdot \nabla) \vec{u} \quad (7)$$

Where  $B$  denotes the flux density and  $u$  the velocity of the melt fluid. The variables  $\mu$  and  $\sigma$  describes the magnetic permeability and electrical conductivity of the melt ( $\mu=1.25e-6\text{H/m}$ ,  $\sigma=1.05e+7\ \Omega^{-1}\text{m}^{-1}$  for liquid Al). It is assumed that the alloy is above the Curie's temperature, so that its magnetic permeability is equal to magnetic permeability of the vacuum. The magnetic field is separated into an exterior, known field  $B_0$  and a secondary, induced field  $b$ , arising from the eddy currents induced in the liquid domain such that  $B = B_0 + b$ . The exterior field  $B_0$  is the field arising from the stirring EMS coils and it can be known from calculations using the coil dimensions and alternating current properties. The Lorentz-forces are calculated from the superposition of magnetic fields  $B_0 + b$  and the induced current density  $j$  by using the relationship:

$$\vec{F} = \vec{j} \times \vec{B} = \vec{j} \times (\vec{B}_0 + \vec{b}) \quad (8)$$

Current density is then obtained using the relationship:

$$\vec{j} = \frac{1}{\mu} \nabla \times \vec{B} \quad (9)$$

This force term in equation (9) is subsequently added into the momentum equations as a source/sink term. The electromagnetic heat released into the melt is given by:

$$Q_{em} = \frac{j^2}{\sigma} \quad (10)$$

This heat released is introduced as a thermal source term in the energy equation. For the present problem, the magnetic Reynold number ( $Re_m = uU\mu\sigma$ ) is low so the induced current caused by the fluid flow was neglected. The magnetic field is calculated together with the flow field using a finite volume CFD-solver (computational fluid dynamics; CFD Fluent with MHD add-on). The simulation method uses the Fluent-specific User Defined Scalar equations. Here, the full coupling between magnetic field and fluid is considered. Boundary conditions for the Maxwell's equations used in calculation of Lorentz force field are as follows:  $\mathbf{J} \cdot \mathbf{n} = 0$  at the walls and the magnetic flux density  $B$  is continuous across the walls. The external magnetic field amplitude was adjusted to obtain

the melt flow velocity strength near the interface same as that obtained using mechanical stirring. The magnetic field frequency was adjusted to get good melt penetration with flow cells close and separate to each other.

## 5 Results and discussions

### 5.1 Mechanical stirring results

The solidification model used in this work was validated elsewhere by Fashu (2011) and Fashu (2016), where the model was tested and compared against experimental results obtained by Lee (2004). There was good agreement between practical compositional results obtained (Fig. 4a) and simulation results (Fig. 4b) showing that the model is capable of computing the solidification process under consideration.

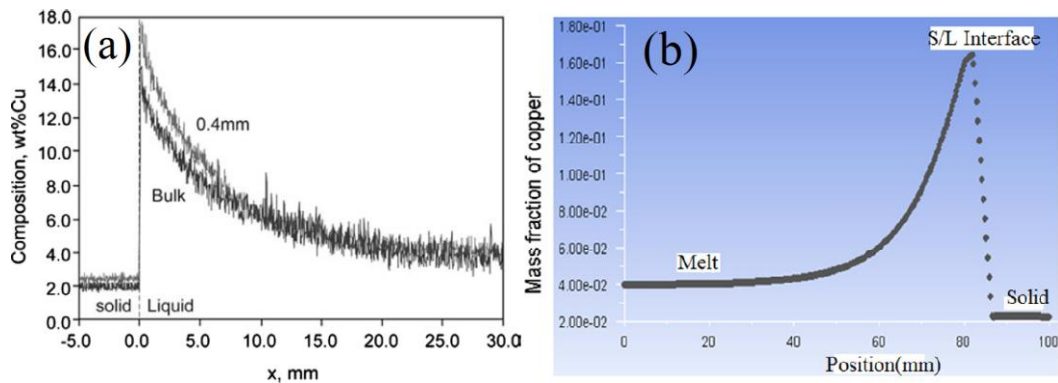


**Figure 4:** Solute redistribution obtained for (a) practical solidification according to Lee (2004) and (b) using the numerical simulation with same experimental conditions in (a) by Fashu (2011) and Fashu (2016).

In mechanical stirring, a stirrer with its propeller blades is positioned in contact with the liquid-solid interface and the liquid phase can be stirred at the same time by the rotation of the blades as shown in Fig.2. The cooling rate of the water spray is carefully adjusted such that the solid-liquid interface will be positioned just at the mold exit. Simulation results in Fig.5 shows the aluminum metal redistribution in the melt, solid-liquid interface and ingot after the OCC process has reached steady state in absence of melt stirring. In accordance with Tiller (1953), the solute redistribution is constant once steady state condition is attained showing that equilibrium between solute rejection and transport into the melt is existing. Fig.6 shows the corresponding axial aluminum redistribution in the melt, solid-liquid interface and ingot. Purification of the ingot occurs during the unsteady transient process before the solute boundary layer is established and once steady state is established, the aluminum ingot purity would be constant and slightly impure compared

with the melt. Reduced ingot purity is due to continuous ejection of the solutes into the melt thereby changing its composition with time and reducing ingot purity but this will occur after casting substantially long ingots.

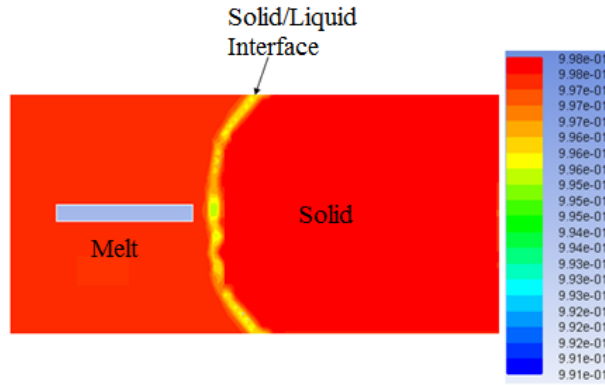


**Figure 5:** Aluminum redistribution at steady state in absence of melt stirring

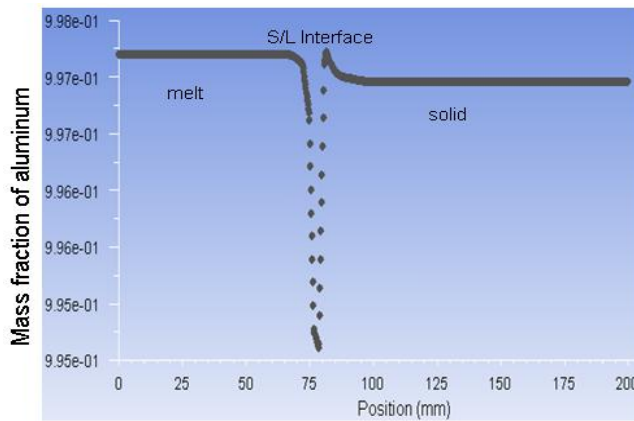


**Figure 6:** Axial distribution of aluminum in absence of melt stirring

The approximate critical stirring intensity required to produce ingots of highest purity during OCC process was obtained through rigorous trial and error simulations using different stirring rates (increasing from zero upwards). Fig. 7 and Fig. 8 shows the solute redistribution in ingot and its corresponding redistribution (near the center) in presence of the optimum melt stirring intensity of 2mm/min for the casting of a 2m long ingot. It is observed that stirring significantly increased the purity of the ingot to above 99.98%Al (Fig.8) from about 99.70% Al (Fig.6). Here aluminium purification mechanism is through breaking down solid extending from the liquid solid interface (mushy zone) into the liquid phase to release impurities from between the dendrites or between the branches of

the dendrites, and dispersing the released impurities in the entire body of the liquid phase as depicted in Fig. 9. Here solute rich fragments are removed from the dendrites and will dissolve into the bulk melt which is maintained at higher temperature. It should also be noted that in addition to transportation of solute rich solids into the bulk melt, solute rich melt in the mushy zone is also transported into the bulk melt and replaced by fresh melt which is not rich in solutes. When aluminium is solidified while dispersing the impurities in the entire body of liquid phase through forced convection, the formation of dendrites at the interface can be inhibited, permitting the melt to solidify while maintaining a smooth interface according to Shingu (1983) and in this way convection will not disturb the flat interface.

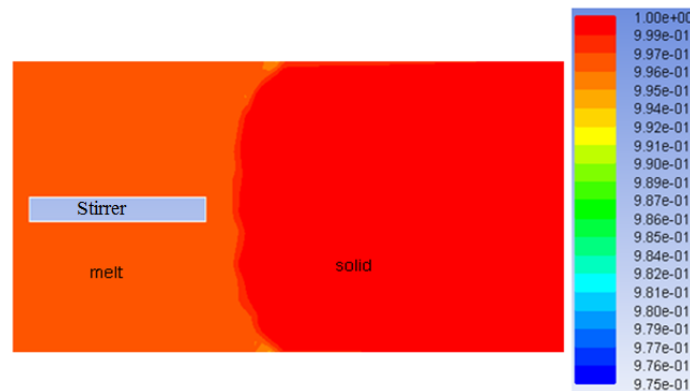


**Figure 7:** Aluminum redistribution in presence of optimum melt stirring intensity of 2mm/min, after casting 2m ingot.

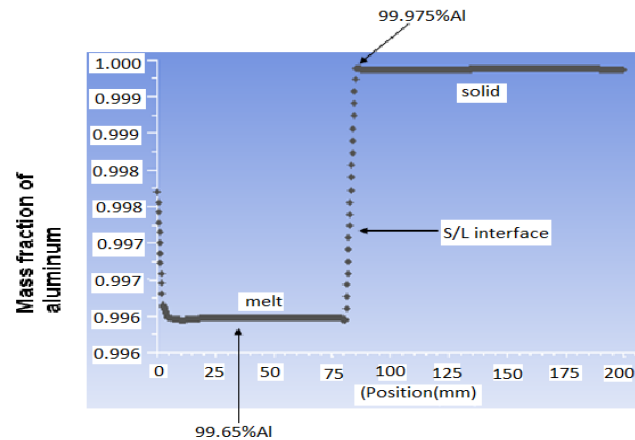


**Figure 8:** Axial aluminum redistribution in melt and ingot in presence of optimum mechanical melt stirring intensity of 2mm/min, after casting 2m ingot.

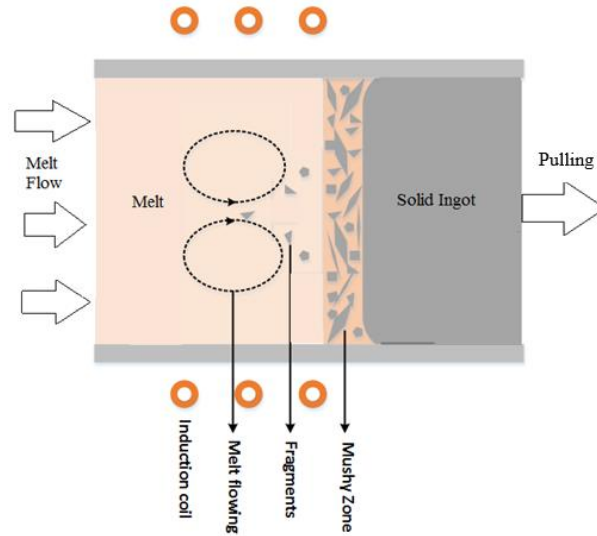


**Figure 9:** Aluminum enrichment mechanism from an interface

The velocity profiles obtained using the optimum mechanical stirring intensity of 2mm/min are shown in Fig.10. The average velocity field distribution near the interface center was approximately 0.015m/s. It is observed that the flow field is a one circular loop following the geometry of the stirrer and the solid-liquid interface at the peripherals is not effectively stirred. In order to improve the velocity flow fields during mechanical stirring, there maybe a need of using many stirrers at different positions near the interface to effectively stir all the regions near the solid-liquid interface and this is complicated and expensive in designing. It is also worth noting that the velocity flow fields are not very strong in the bulk melt away from the stirrer locus and such weak mixing is disadvantageous for solute transport.

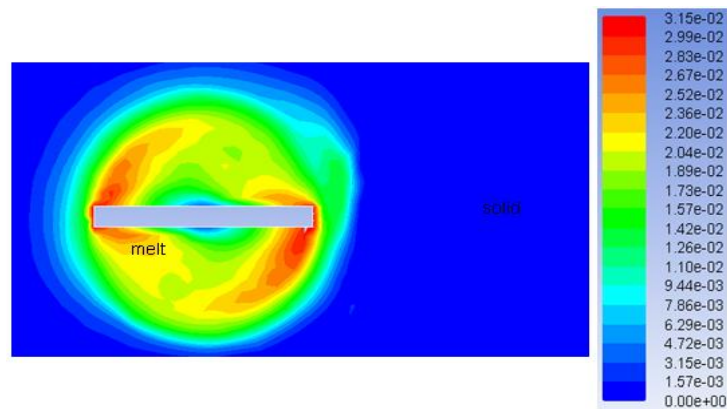
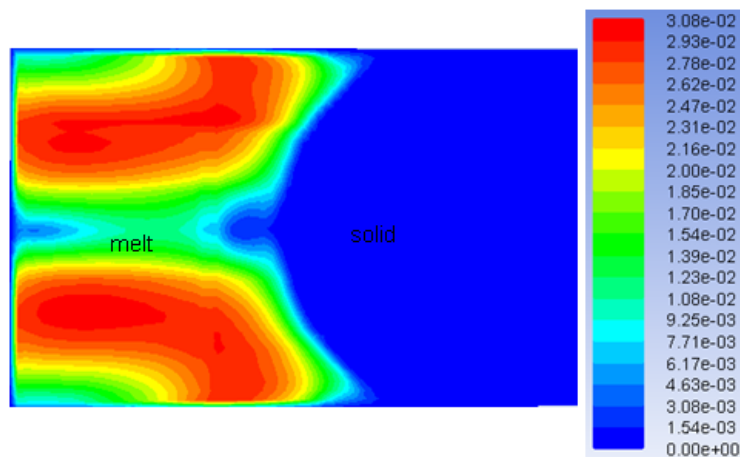


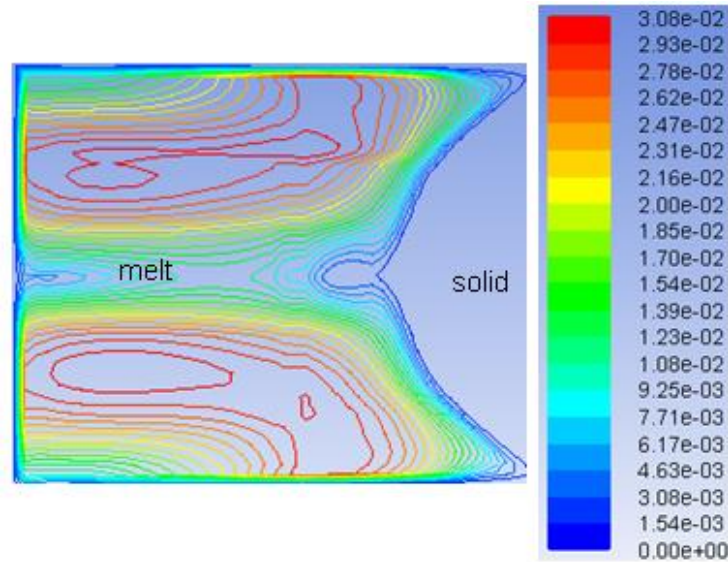
**Figure10:** Velocity profile in m/s for optimum mechanical melt stirring of 2mm/min

### 5.2 Electromagnetic stirring results

Numerical simulation to study the influence of frequency and magnetic induction on flow field was performed and after a rigorous systematic changing of parameters it was found that at a frequency of  $f=2.7$  Hz and a magnetic induction of  $B_0=20$ mT an average velocity field of 0.0154m/s was produced near the solid-liquid interface as shown in Fig.11. This magnitude of the average velocity flow field is close to that for the optimum mechanical stirring determined in **section 5.1** which was approximately 0.015m/s on average. Here, it is observed that the electromagnetic stirring produced two axial convective loops perpendicular to the solid-liquid interface while stirring the melt and it effectively stir all the regions near the solid-liquid interface. A previous research by Fashu (2016), Noeppl (2010), Chen (2014) and Ma (2006) has shown that axial stirring of the melt is stronger than tangential stirring and more effective in thinning the solute boundary layer. Moreover, the results in Fig.11 also show that the frequencies required to produce optimum velocity flow fields are very small, yet they produce good penetration of the melt and a small body force which is just enough to eliminate the solute boundary layer as required. Although the velocity profiles near the solid-liquid interface are the same as those produced by mechanical stirring (Fig.10), the velocity magnitudes produced by electromagnetic stirring in the bulk melt are larger than those produced by mechanical stirring. This likely produces better mixing for efficient transport of solutes thereby producing substantially longer, uniform and higher purity ingots than those produced from mechanical stirring for a long time.



(a)



(b)

**Figure 11:** Computed velocity field for  $B_0 = 20$  mT and  $f=2.7$ Hz. (a) Magnitude of the azimuthal velocity in m/s. (b) Streamlines of the meridian recirculation for optimum electromagnetic stirring.

Analysis of the segregation in the aluminum ingot produced by electromagnetic stirring is shown in Fig.12 and show that axial (central) solutes fields in the ingot obtained are almost the same as those obtained from mechanical stirring (Fig. 7), except for a slight increase in ingot purity and slight decrease in melt aluminum content. This is likely to be due to uniform and consistent solute transport in electromagnetic stirring compared to mechanical stirring as explained before in the discussion of Fig.11. It should be noted here that although the analysis of the solute fields was only done on the central part of the ingot, the purity of the ingots on the periphery during electromagnetic stirring is expected to be higher than that for mechanical stirring due to effective stirring in magnetic stirring as shown in velocity profiles in Fig.10 and Fig.11.

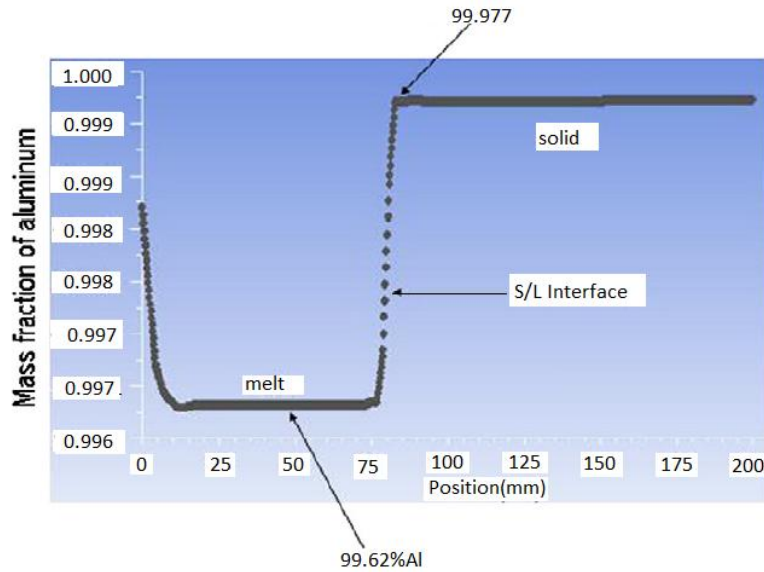


**Figure12:** Axial aluminum redistribution in melt and ingot in presence of optimum electromagnetic melt stirring intensity of  $B_0 = 20$  mT and  $f=2.7$ Hz.

Using the computed magnetic field parameters (frequency and strength), the current and frequency of a specific stirrer can be determined and the magnetic stirrer can be designed analytically. The current intensity  $I$ , required can be calculated using the relationship:

$$B = \frac{1}{2} \mu NI \left( \frac{1}{\sqrt{L^2 + R^2}} \right) \quad (11)$$

Where,  $B$  is the induced magnetic flux density,  $\mu$  is the magnetic permeability,  $N$  is the number of the coil windings,  $I$  is the current,  $L$  is the length of the coil and  $R$  is the radius of the solenoid. The frequency of the alternating current induced in the coil can be known from the relation:  $\omega = 2\pi f$ , where  $f$  is the frequency of the alternating current.

### 5.2.1 Validation of the magnetic stirring model

The capability of the CFD Fluent 6.3.26 magnetic induction method used to predict electromagnetic stirring during OCC process can be validated by comparing against the results obtained by Armour (2008) which are shown in Fig.13, where electromagnetic melt stirring was used. Comparing the result of flow fields in Fig. 13 with our results in

Fig.11 show that the velocity profiles (in terms of orientation) obtained are in good agreement (as is expected of streamlines during electromagnetic stirring), demonstrating that the Fluent code used here is capable and valid in predicting electromagnetic stirring of the designed stirrer. In addition to this comparison, Noepfel (2010) also obtained similar velocity flow fields during casting of binary Al-alloys in presence of electromagnetic stirring.

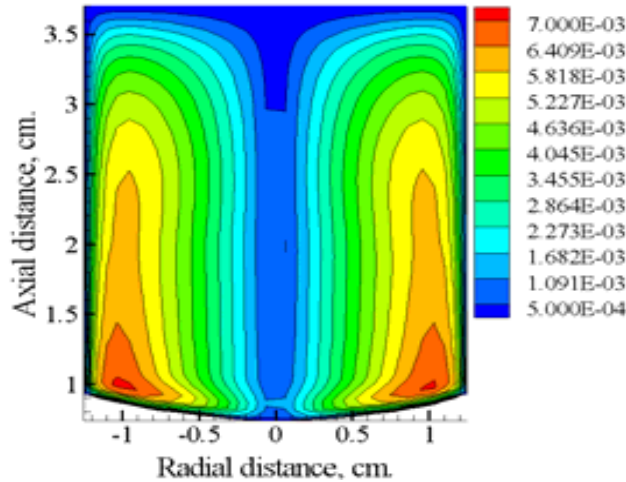


**Figure 13:** CFX flow field for  $f = 10$  Hz and  $B = 2.0$  mT obtained by Armour (2008)

## 6 Conclusions

With the purpose of purifying an industrial aluminum alloy during Ohno continuous casting, the use of mechanical and electromagnetic melt stirring techniques was compared. The optimum stirring parameters (mechanical and electromagnetic) for effectively stirring were determined. The following conclusions can be drawn:

1. To produce an almost similar optimum velocity flow field required for high purity ingots, an optimum stirring rate of 2mm/min was determined for mechanical stirring and the optimum magnetic field with an amplitude of 20mT and a frequency of 2.7Hz was predicted for electromagnetic stirring.
2. The distribution of the velocity pattern near the solid-liquid interface was more uniform and covered the entire region in electromagnetic stirring when compared to mechanical stirring showing that magnetic stirring was effective in producing homogeneous ingots of higher purity.
3. Electromagnetic stirring can produce substantially longer ingots of higher purity than mechanical stirring since it was more efficient in bulk melt mixing for solute transport

compared to mechanical stirring.

**Acknowledgement** We greatly appreciate support from the Harare Institute of Technology in providing the facilities used to carry this work.

## References

- Adler, K.; Schwarze, R.; Galindo, V.** (2005): Numerical Modeling of the Evaporation Process of an Electromagnetically Stirred Copper Melt. *In FLUENT CFD Forum*.
- Amour, N.; Yildiz, M. ; Yildiz, E. ; Dost, S.** (2008): Liquid phase diffusion growth of SiGe single crystals under magnetic fields. *ECS Transactions.*, vol.16, pp.135-146.
- Ban, B.; Li, Y.; Zuo, Q.; Zhang, T.; Chen, J.; Dai, S.** (2015): Refining of metallurgical grade Si by solidification of Al–Si melt under electromagnetic stirring. *Journal of Materials Processing Technology.*, vol.222, pp.142-147.
- Bennon, W.; Incropera, F.** (1987): A continuum model for momentum, heat and species transport in binary solid-liquid phase change systems—I. Model formulation. *International Journal of Heat and Mass Transfer.*, vol. 30, pp.2161-2170.
- Cablea, M.; Zaidat, K.; Gagnoud, A.; Nouri, A.; Chichignoud, G.; Delannoy, Y.** (2015): Multi-crystalline silicon solidification under controlled forced convection. *Journal of Crystal Growth.*, vol.417, pp. 44-50.
- Chen, J.C.; Chiang, P.Y.; Chang, C.H.; Teng, Y.Y.; Huang, C.C.; Chen, C.H; Liu, C.C.** (2014): Three-dimensional numerical simulation of flow, thermal and oxygen distributions for a Czochralski silicon growth with in a transverse magnetic field. *Journal of Crystal Growth.*, vol.401, pp.813-819.
- Dumitrica, S.; Vizman, D.; Garandet, J.P.; Popescu, A.** (2012): Numerical studies on a type of mechanical stirring in directional solidification method of multicrystalline silicon for photovoltaic applications. *Journal of Crystal Growth*, vol. 360, pp.76-80.
- Eckert, S.; Nikrityuk, Petr.A.; Räßiger, D.; Eckert, K.; Gerbeth,G.** (2007): Efficient melt stirring using pulse sequences of a rotating magnetic field: part I. Flow field in a liquid metal column. *Metallurgical and Materials Transactions B.*, vol.38, pp.977-988.
- Fashu, S.; Jianguo, L.; Hu, Q.D.** (2011): Purification of an industrial aluminum alloy by melt stirring during ohno continuous casting process. *Materials Letters.*, vol. 65, pp. 2248–2250.
- Fashu, S.; Khan, R.** (2016): Comparison between axial and radial melt stirring on purification of industrial aluminum during Ohno Continuous Casting, *Engineering Science and Technology an International Journal.*, vol.19, pp.2100-2108.

**Jie, J.C.; Zou, Q.C.; Wang, H.W.; Sun, J.L.; Lu, Y.P.; Wang, T.M.; Li, T.J.** (2014): Separation and purification of Si from solidification of hypereutectic Al–Si melt under rotating magnetic field. *Journal of Crystal Growth.*, vol.399, pp.43-48.

**Lee, J. H.; Shan, I.; Miyahara, H.; Trivedi, R.** (2004): Diffusion coefficient measurement in liquid metallic alloys, *Metall. Trans. B.*, vol.35, pp.909–917.

**Li, M.; Tamura, T.; Omura, N.; Murakami, Y.; Tada, S.** (2016): Grain refinement of AZCa912 alloys solidified by an optimized electromagnetic stirring technique. *Journal of Materials Processing Technology.*, vol. 235, pp.114-120

**Li, X.; Guo, Z.; Zhao, X.; Wei, B.; Chen, F.; Li, T.** (2007): Continuous casting of copper tube billets under rotating electromagnetic field. *Materials Science and Engineering A.*, vol.460, pp.648-651.

**Ma, N.; Walker, J.S.** (2006): Electromagnetic stirring in crystal growth processes. *FDMP: Fluid Dynamics & Materials Processing.*, vol.2, pp.119-126.

**Mapelli, C.; Gruttadauria, A.; Peroni, M.** (2010): Application of electromagnetic stirring for the homogenization of aluminium billet cast in a semi-continuous machine. *Journal of Materials Processing Technology.*, vol.210, pp.306-314.

**Marcelo, J.; Colaco, I.; Dulikravich, G.** (2007): Solidification of double-diffusive flows using thermo-magneto-hydrodynamics and optimization. *Materials and Manufacturing Processes.*, vol. 22, pp.594-606.

**Marcelo, J.; Colaco, I.; Dulikravich, G.** (2003): Reducing convection effects in solidification by applying magnetic fields having optimized intensity distribution. In ASME 2003 Heat Transfer Summer Conference. *American Society of Mechanical Engineers.*, pp.199-209.

**Metan, V.; Eigenfeld, K.; Rübiger, D.; Leonhardt, M.; Eckert, S.** (2009): Grain size control in Al–Si alloys by grain refinement and electromagnetic stirring. *Journal of alloys and compounds.*, vol.487, pp.163-172.

**Mitric, A.; Duffar, T.** (2008): Design of vertical Bridgman experiments under alternating magnetic field. *Journal of Crystal Growth.*, vol.310, pp.1511-1517.

**Motoyasu, G.; Yamazaki, H.; Ohno, A.; Soda, H.; McLean, A.** (2015): Some Perspectives on Innovative Processing and Materials Development. *Journal of Materials Engineering and Performance.*, vol.24, pp.2240-2249.

**Mullin, J.; Hulme, K.** (1958): The Use of Electromagnetic Stirring in Zone Refining. *International Journal of Electronics.*, vol.4, pp.170-174.

**Noepfel, A.; Ciobanas, A.; Wang, X.D.; Zaidat, K.; Mangelinck, N.; Budenkova, O.;**

**Weiss, A.; Zimmermann, G.; Fautrelle, Y.**(2010): Influence of forced/natural convection on segregation during the directional solidification of Al-based binary alloys. *Metall. Trans. B.*, vol 41, pp. 193-208.

**Ohno, A.** (1986): Continuous casting of single crystal ingots by the OCC process. *Journal of Metals.*, vol.38, pp.14-16.

**Okayasu, M.; Takasu, S.; Yoshie, S.** (2010): Microstructure and material properties of an Al–Cu alloy provided by the Ohno continuous casting technique. *Journal of Materials Processing Technology.*, vol.210, pp.1529-1535.

**Okayasu, M.; Yoshie, S.** (2010): Mechanical properties of Al–Si 13–Ni 1.4–Mg 1.4–Cu 1 alloys produced by the Ohno continuous casting process. *Materials Science and Engineering A.*, vol.527, pp.3120-3126.

**Shingu, H.; Arai, K.; Ootsuka, R.; Showa Aluminium Kabushiki Kaisha.** (1983): Process of preparing aluminum of high purity. *U.S. Patent.*, 4,373,950.

**Tiller, W.; Jackson, K.; Rutter, J.; Chalmers, B.** (1953): The redistribution of solute atoms during the solidification of metals. *Acta Metallurgica.*, vol.1, pp. 428-437.

**Wang, Y.H.; Xiao, L.R.; Zhao, X.J.; Hu, W.; Song, Y.F.; Zhang, W.; Zhou, H.** (2015): Microstructure and mechanical properties of columnar-grained copper produced by the Ohno continuous casting technique. *Materials Science and Engineering A.*, vol. 639, pp.122-130.

**Willers, B.; Eckert, S.; Nikrityuk, P.A.; Rübiger, D.; Dong, J.; Eckert, K.; Gerberth, G.** (2008): Efficient melt stirring using pulse sequences of a rotating magnetic field: Part II. Application to solidification of Al-Si alloys. *Metallurgical and Materials Transactions B.*, vol.39, pp.304-316.

**Yu, W.; Ma, W.; Lv, G.; Xue, H.; Li, S.; Dai, Y.** (2014): Effect of electromagnetic stirring on the enrichment of primary silicon from Al–Si melt. *Journal of Crystal Growth.*, vol.405, pp.23-28.

**Yu, W.; Ma, W.; Zheng, Z.; Lei, Y.; Jiang, W.; Li, J.** (2017): Si Purification by Removal of Entrapped Al during Electromagnetic Solidification Refining of Si-Al Alloy. *Metallurgical and Materials Transactions B.*, vol.48, pp.1-8.

**Zeng, J.; Chen, W.; Yan, W.; Yang, Y.; McLean, A.** (2016): Effect of permanent magnet stirring on solidification of Sn-Pb alloy. *Materials & Design.*, vol.108, pp. 364-373.